J Electr Eng Technol Vol. 8, No. 5: 1029-1039, 2013
http://dx.doi.org/10.5370/JEET.2013.8.5.1029

ISSN(Print) 1975-0102
ISSN(Online) 2093-7423

Design and Evaluation of a Protection Relay for a Wind Generator Based on the Positive- and Negative-Sequence Fault Components

Taiying Zheng*, Seung-Tae Cha, Yeon-Hee Kim*, Peter A. Crossley***, Sang Ho Lee§ and Yong Cheol Kang†**

Abstract – To avoid undesirable disconnection of healthy wind generators (WGs) or a wind power plant, a WG protection relay should discriminate among faults, so that it can operate instantaneously for WG, connected feeder or connection bus faults, it can operate after a delay for inter-tie or grid faults, and it can avoid operating for parallel WG or adjacent feeder faults. A WG protection relay based on the positive- and negative-sequence fault components is proposed in the paper. At stage 1, the proposed relay uses the magnitude of the positive-sequence component in the fault current to distinguish faults requiring non-operation response from those requiring instantaneous or delayed operation responses. At stage 2, the fault type is first determined using the relationships between the positive- and negative-sequence fault components. Then, the relay differentiates between instantaneous operation and delayed operation based on the magnitude of the positive-sequence fault component. Various fault scenarios involving changes in position and type of fault and faulted phases are used to verify the performance of the relay. This paper concludes by implementing the relay on a hardware platform based on a digital signal processor. Results indicate that the relay can successfully distinguish the need for instantaneous, delayed, or non-operation.

Keywords: Wind generator protection, Outage zone minimization, Instantaneous operation, Delayed operation, Non-operation, Symmetrical components

1. Introduction

To reduce the emission of greenhouse gases, the Kyoto Protocol on climate change represents a significant political and environmental international regimen [1]. Many countries are attempting to integrate increased amounts of renewable energy, such as wind, solar, bio-, and hydraulic energy, into their electrical networks, not only to meet the increasing demand for energy, but also to meet environmental goals. In addition, the World Wide Fund for Nature has released "The Energy Report [2]" outlining how the world can be powered by 100% renewable energy by 2050.

Among these renewable energy resources, wind energy has become the most promising alternative due to its significant technical advances and demonstrated financial viability over the last decade. The installed capacity of wind generators (WGs) reached 196.6 GW at the end of 2010, producing 430 TWh to the worldwide electricity supply [3]. In addition, a large-scale off-shore wind power plant (WPP) has been built to minimize production cost and adverse effects on the power system operation and stability. Korea has begun construction of a 2.5 GW off-shore WPP on the western coast expected to complete in 2019.

As the penetration level of wind energy increases, more reliable protection systems for WGs and WPPs are required. Techniques for protecting a small WPP have been reported [4-6]. A source-based protection relay using a shaped directional operating characteristic was proposed in [4, 5]. The performance of a mho relay was quantitatively analyzed based on a sensitivity model for its operation margin [6]. These relays were installed at the point of common coupling, and with these if a fault occurred in the WPP, the entire plant would be disconnected.

Conventional protection relays for an individual WG were numerated [7, 8]. These methods employ over/under voltage, over/under frequency, instantaneous phase/neutral over-current for generator phase/ground faults, and inverse time phase over-current for generator overload. They can successfully protect a WG when an internal fault occurs. However, they are unable to detect a collector feeder fault or a collector bus fault and distinguish them from an inter-tie fault or a grid fault. In addition, they cannot distinguish between a connected feeder fault and an adjacent feeder

† Corresponding Author: Dept. of Electrical Engineering and WeGAT Research Centre, and Smart Grid Research Centre, Chonbuk National University, Chonju, Korea. (yckang@jbnu.ac.kr)
* Dept. of Electrical Engineering and Wind energy Grid-Adaptive Technology (WeGAT) Research Centre, Chonbuk National University, Chonju, Korea. (huanxiong417@hotmail.com, love35021@jbnu.ac.kr)
** Dept. of Electrical Engineering, Technical University of Denmark, Denmark. (stc1405@gmail.com)
*** School of Electrical and Electronic Engineering, University of Manchester, UK. (peter.crossley@manchester.ac.uk)
§ Korea Electrotechnology Research Institute, Korea. (sanghlee@keri.re.kr)
Received: April 16, 2013; Accepted: June 10, 2013

fault. Thus, the outage zone can be wider than is necessary or desirable.

When a fault occurs, the outage zone should be minimized; this increases the availability of the WGs and reduces the negative impact on grid stability. To achieve this objective, the WG protection relay should operate instantaneously for a WG fault, connected feeder fault, or collection bus fault, and it should operate after a delay for an inter-tie fault or grid fault. In addition, the relay should remain stable for a fault on a parallel WG connected to the same feeder and for an adjacent feeder fault.

A WG protection algorithm using the magnitude of the positive-sequence fault component and the phase angle of the negative-sequence fault component was proposed [9]. The phase angle of the negative-sequence fault component is used to distinguish the fault type i.e., a single line-to-ground (SLG) fault or a three-phase (3P) fault; and then the magnitude of the positive-sequence fault component is used to decide if instantaneous operation or delayed operation is required. However, the algorithm can distinguish fault types into only the two types, i.e. an SLG or 3P.

The basic idea of a WG protection algorithm based on the fault-generated symmetrical components was proposed [10]. The proposed algorithm is composed of two stages. At stage 1, the magnitude of the positive-sequence fault component is used to discriminate a fault on a parallel WG connected to the same feeder, or on an adjacent feeder, from the other faults requiring an instantaneous or delayed tripping response. At stage 2, the algorithm employs an instantaneous directional algorithm using the positive-sequence fault components to discriminate short-circuit faults internal to the generator from other faults. The type of fault is first evaluated using the relationships between the positive- and negative-sequence fault components. Then the magnitude of the positive-sequence fault component is used to decide between instantaneous or delayed operation. This paper describes the results of the extensive study of the WG protection algorithm [10]. The derivation of relationship between the fault-generated symmetrical components is included in this paper for fault type identification. To verify the performance of the proposed relay, various fault scenarios involving changes in the position and type of fault and the phases involved in the fault are modelled using an EMTP-RV simulator. In addition, this paper concludes by implementing the proposed relay into a hardware platform based on a TMS320C6701 digital signal processor (DSP).

2. WPP Model and WG Relay Functions

2.1 Configuration of a WPP

Fig. 1 shows a model of the 100 MW WPP studied in this paper. Ten medium voltage (MV) power collection

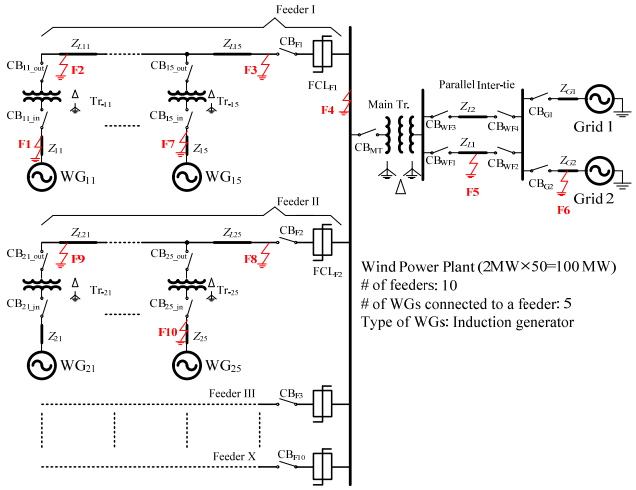

Fig. 1. WPP model

Table 1. Required relay functions for WG_{11} to minimize an outage zone

Fault positions	Fault types	Required relay operation
F1-F4	SLG, LL, DLG, 3P	Instantaneous operation
F5-F6		Delayed operation
F7-F10		Non-operation

feeders (22.9 kV) are connected to a collector bus, which is connected to the strong grid (345 kV) through a main transformer, substation bus, and parallel inter-tie lines. Five induction generators, each rated at 2 MW, are connected to each feeder through step-up transformers. All WGs are fixed-speed asynchronous squirrel-cage induction generators.

In this paper, a fault current limiter (FCL) is assumed to be installed beside a circuit breaker (CB) on each feeder, as shown in Fig. 1. The reason is as follows. Although the grounding impedance of the main transformer can limit the fault current for an SLG or double line-to-ground (DLG) fault, it is not effective for a line-line (LL) or 3P fault. Therefore, FCLs are often used in a large WPP to limit the fault current [11, 12].

The characteristics of a fault current depend on the winding connection of a step-up transformer and substation transformer. A grounded-wye-delta transformer is used as a step-up transformer in a WG. This is because the delta connection provides isolation of a WG from the zero-sequence behavior of the collector feeder, and the grounded-wye connection provides a solid ground for the low-voltage side of the WG [13]. A grounded-wye-grounded-wye transformer with a delta tertiary, which is mostly used as a substation transformer [14], is modeled in this paper.

2.2 Required WG relay functions

This subsection describes the WG (i.e., WG_{11}, connected to Feeder I) protection relay's functions to minimize an outage zone. Table 1 shows the functions that the WG

protection relay should have. The cases F1-F10 illustrated in Fig. 1 show the fault positions.

F1 depicts a case of an internal fault of the WG_{11}, while F2 and F3 depict cases of connected feeder faults. F4 depicts a collector bus fault. In the cases F1-F4, the relay for the WG_{11} should operate instantaneously.

F5 depicts an inter-tie fault. In this case, the WG relay operation depends on the configuration of the inter-tie, single-, or multiple-lines. The relay for WG_{11} for a single-line should operate instantaneously. However, for multiple-lines, the relay should detect the fault and operate with a delay. In this paper, the configuration of the inter-tie assumes multiple-lines, which is necessary for a large WPP. Thus, the WG relay should operate with a delay. The delay time should be determined considering the coordination time between the corresponding relays.

F6 indicates a grid fault, which is located far from a WG. Modern grid codes in many countries require that a WG or WPP protection relay should have a low voltage ride-through (LVRT) capability in this case. Therefore, the WG relay should be carefully designed to have LVRT capability that considers the grid codes of each country.

F7 depicts an internal fault on another WG (WG_{15}) connected to the same feeder. In this situation, the relay for WG_{15} should operate instantaneously, while the relay for WG_{11} should not operate. F8-F10 depict adjacent feeder faults, including an internal fault of a WG connected to an adjacent feeder, for which the relay for WG_{11} should not operate.

3. Protection Relay for a WG based on Positive- and Negative-sequence Fault Components

This paper uses the fault component of the current at the relaying point, which is defined as the fault-generated current, instead of the measured current at the relaying point. The fault component of the current at the relaying point is obtained by subtracting the load current from the measured current after the fault inception. It can be assumed that the magnitude of the load current during a very short period (e.g., two or three cycles) after the fault inception remains the same as that prior to the fault. In this paper, the fault component of the current is calculated by subtracting the load current from the measured current at the relaying point during the fault, as in [15].

The proposed algorithm is composed of two stages. At stage 1, the magnitude of a positive-sequence fault component is used to distinguish F7-F10 faults from F1-F4 and F5/F6 faults. At stage 2, F1-F4 faults are distinguished from F5/F6 faults. First, the fault direction is discriminated using an instantaneous directional algorithm based on the positive-sequence fault components to distinguish F1 faults (forward faults) from F2−F4 and F5/F6 faults (backward faults). Then, the type of fault, i.e., SLG, LL, DLG, or 3P, is evaluated using the relationships between the positive- and negative-sequence fault components, which depend on the type of fault. Finally, the magnitude of the positive-sequence fault component is used to decide on either instantaneous operation (F2-F4 faults) or delayed operation (F5/F6 faults).

3.1 Stage 1: Distinguishing F7-F10 faults (Non-operation) from F1-F4 and F5/F6 faults (Instantaneous or delayed operation)

In this stage, the magnitude of a positive-sequence fault component is used to distinguish faults at F7-F10 from those at F1-F4 and F5/F6. When a fault occurs at F7-F10, the relay for a WG connected to the healthy feeder would "see" the fault through its step-up transformer and the FCL installed at the faulted feeder. The impedance seen for the fault from the WG is so large that the fault current flowing out is limited to a small value, which is similar to a normal load current. The threshold K_{ini} can be decided based on fault analysis of the studied system.

On the other hand, the relay for another WG connected to the faulted feeder would "see" the fault only through its step-up transformer. For this reason, the magnitude of a positive-sequence fault component is increased significantly.

Consequently, an internal fault of another WG connected to the same feeder or an adjacent feeder, for which the relay should not operate, can be discriminated successfully based on the magnitude of the positive-sequence fault component.

3.2 Stage 2: Distinguishing F1-F4 faults (Instantaneous operation) from F5/F6 faults (Delayed operation)

In this stage, the proposed relay discriminates F1-F4 faults (instantaneous operation) from F5/F6 faults (delayed operation). Among these faults, only F1 faults are forward faults while the other faults, i.e., F2−F4 and F5/F6 faults, are backward faults. To do this, a directional algorithm based on the positive-sequence fault components [15] is used.

For a forward fault, the phase relationship between the positive-sequence fault components at the relay location is:

$$\theta_{direction} = \angle \boldsymbol{V}_{Raf}^{+} - \angle \boldsymbol{I}_{Raf}^{+} \approx -90^{\circ}, \quad (1)$$

where $\boldsymbol{V}_{Raf}^{+}$ and $\boldsymbol{I}_{Raf}^{+}$ are the positive-sequence fault components.

For a backward fault, the phase relationship is:

$$\theta_{direction} = \angle \boldsymbol{V}_{Raf}^{+} - \angle \boldsymbol{I}_{Raf}^{+} \approx 90^{\circ}. \quad (2)$$

Considering the errors involved in the measuring process and the sensitivity of the relay, the criteria for a forward fault and backward fault are set as:

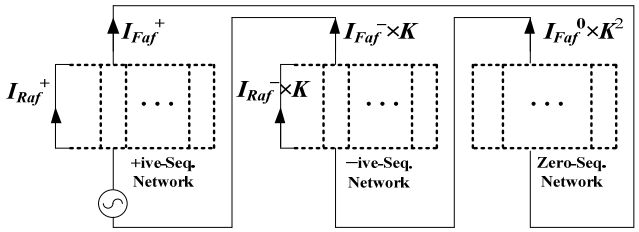

(a) Sequence-network connection for an SLG fault

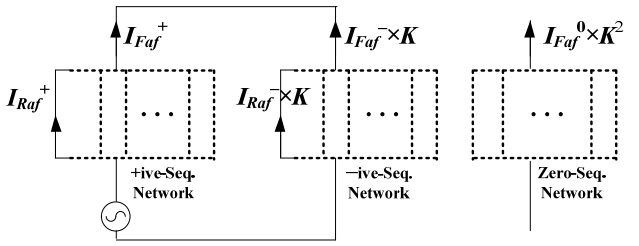

(b) Sequence-network connection for an LL fault

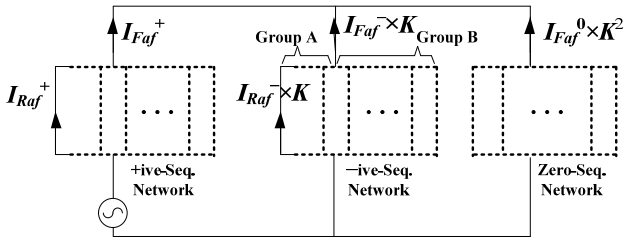

(c) Sequence-network connection for a DLG fault

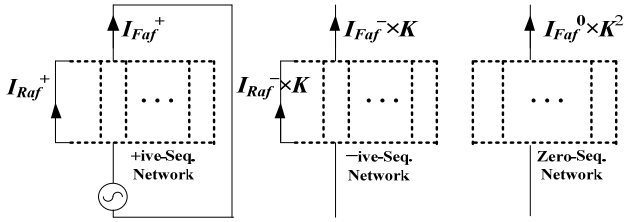

(d) Sequence-network connection for a 3P fault

Fig. 2. Sequence-network connections for four fault types

$$-180° + \delta \le \theta_{direction} \le -\delta \quad (3)$$

$$\delta \le \theta_{direction} \le 180° - \delta, \quad (4)$$

where δ, the blocking angle, is set to be 30° in this paper.

The magnitude of a fault current depends on the distance from the relaying point for the same type of fault. However, a fault current of a 3P fault at a distant location can be larger than that of an LL fault at a closer position. For example, the fault current for the F5_3P fault can be larger than that of F4_LL fault. Thus, to decide whether the fault from the relaying point is far or close, fault type classification is necessary. In this paper, the fault type is evaluated first to clearly discriminate F2-F4 faults (instantaneous operation) from F5/F6 faults (delayed operation).

Conventionally, the zero-sequence current has been used to distinguish the grounded fault and phase-to-phase fault. However, it is unable to evaluate the four kinds of fault types, i.e., SLG, LL, DLG, and 3P. In addition, the zero-sequence current does not flow through the relaying point due to the grounded-wye-delta connection of the step-up transformer of a WG, as shown in Fig. 1.

Thus, in this paper, an algorithm to evaluate the type of fault based on the positive- and negative-sequence fault components at the relaying point is proposed. Fig. 2 shows the sequence-network connections for four types of faults. In Fig. 2, a solid line indicates the corresponding WG and a dotted line indicates the other WGs, collector feeder, and transmission system.

3.2.1 For an SLG fault

In Fig. 2a, $\boldsymbol{I}_{Raf}^{+}$ and $\boldsymbol{I}_{Raf}^{-}$ are the positive- and negative-sequence fault components at the relaying point, respectively. $\boldsymbol{I}_{Faf}^{+}$, $\boldsymbol{I}_{Faf}^{-}$, and $\boldsymbol{I}_{Faf}^{0}$ are the positive-, negative-, and zero-sequence fault components at the fault point, respectively. It is well known that the relationship between the symmetrical components of the fault current at the fault point is:

$$\boldsymbol{I}_{Faf}^{+} = \boldsymbol{I}_{Faf}^{-} \times \boldsymbol{K} = \boldsymbol{I}_{Faf}^{0} \times \boldsymbol{K}^2, \quad (5)$$

where $\boldsymbol{K}$ is 1, $1\angle -120°$ or $1\angle 120°$ for the faulted phase of phase A, phase B, and phase C, respectively. Phase A is selected as a reference frame [16].

From the positive- and negative-sequence networks, the relationships between the fault components of the relaying point and the fault point are:

$$\boldsymbol{I}_{Raf}^{+} = \boldsymbol{K}_{+} \times \boldsymbol{I}_{Faf}^{+} \quad (6)$$

$$\boldsymbol{I}_{Raf}^{-} = \boldsymbol{K}_{-} \times \boldsymbol{I}_{Faf}^{-}, \quad (7)$$

where both $\boldsymbol{K}_{+}$ and $\boldsymbol{K}_{-}$ are vector coefficients that depend on the positive- and negative-sequence networks. It can be assumed that $\boldsymbol{K}_{+}$ equals $\boldsymbol{K}_{-}$, since the positive- and negative-sequence networks have the same topology.

From (5-7), the relationship between the positive- and negative-sequence fault components at the relaying point can be given as:

$$\boldsymbol{I}_{Raf}^{+} = \boldsymbol{I}_{Raf}^{-} \times \boldsymbol{K} \quad (8)$$

Eq. (8) can be rewritten in terms of magnitude and phase angle as:

$$\left|\boldsymbol{I}_{Raf}^{+}\right| = \left|\boldsymbol{I}_{Raf}^{-}\right|\left|\boldsymbol{K}\right| = \left|\boldsymbol{I}_{Raf}^{-}\right| \quad (9)$$

$$\angle \boldsymbol{I}_{Raf}^{+} = \angle \boldsymbol{I}_{Raf}^{-} + \angle \boldsymbol{K} \quad (10)$$

Considering the phase angle shift (60°) of a step-up

transformer, the phase angle difference (θ_{diff}) can be represented by:

$$\theta_{diff} = \angle \boldsymbol{I}_{Raf}^{+} - \angle \boldsymbol{I}_{Raf}^{-} = 60°, -60° \text{ or } 180° \quad (11)$$

In conclusion, when an SLG fault occurs at F2−F6, $|\boldsymbol{I}_{Raf}^{+}|$ is equal to $|\boldsymbol{I}_{Raf}^{-}|$, and θ_{diff} is 60°, −60°, or 180°, depending on the faulted phase.

3.2.2 For an LL fault

In Fig. 2b, the relationship between the symmetrical components of the fault current for an LL fault is given by:

$$\boldsymbol{I}_{Faf}^{+} + \boldsymbol{I}_{Faf}^{-} \times \boldsymbol{K} = 0 , \quad (12)$$

where $\boldsymbol{K}$ is 1, $1\angle$-120°, or $1\angle 120°$ for a B-C-phase, C-A-phase, or A-B-phase LL fault, respectively.

The relationships between the fault components of the relaying point and the fault point are the same as (6) and (7). Substituting (6) and (7) into (12) gives:

$$\boldsymbol{I}_{Raf}^{+} + \boldsymbol{I}_{Raf}^{-} \times \boldsymbol{K} = 0 . \quad (13)$$

Eq. (13) can be interpreted as:

$$\left|\boldsymbol{I}_{Raf}^{+}\right| = \left|\boldsymbol{I}_{Raf}^{-}\right|\left|\boldsymbol{K}\right| = \left|\boldsymbol{I}_{Raf}^{-}\right| \quad (14)$$

$$\angle \boldsymbol{I}_{Raf}^{+} = \angle \boldsymbol{I}_{Raf}^{-} + 180° + \angle \boldsymbol{K} . \quad (15)$$

Considering the phase angle shift effect of a step-up transformer, θ_{diff} can be calculated by:

$$\theta_{diff} = \angle \boldsymbol{I}_{Raf}^{+} - \angle \boldsymbol{I}_{Raf}^{-} = 180°, 60° \text{ or } -60° \quad (16)$$

In conclusion, when an LL fault occurs at F2−F6, $|\boldsymbol{I}_{Raf}^{+}|$ is equal to $|\boldsymbol{I}_{Raf}^{-}|$, and θ_{diff} is −120°, 120°, or 0°, depending on the faulted phase.

3.2.3 For a DLG fault

For a DLG fault, the relationship between the symmetrical components of the fault current can be given by:

$$\boldsymbol{I}_{Faf}^{+} + \boldsymbol{I}_{Faf}^{-} \times \boldsymbol{K} + \boldsymbol{I}_{Faf}^{0} \times \boldsymbol{K}^2 = 0 , \quad (17)$$

where $\boldsymbol{K}$ is 1, $1\angle$-120°, or $1\angle 120°$ for a B-C-phase, a C-A-phase, or an A-B-phase DLG fault, respectively.

The zero-sequence component of the fault current at the relaying point does not exist due to the connection of a step-up transformer. Thus, (17) cannot be used directly.

For a zero-sequence network, the equivalent impedance can be approximated as that of an FCL.

The negative-sequence network is composed of parallel connection of two groups, i.e., group A and group B in Fig. 2c. The equivalent impedance of group A depends on the number of included WGs, and it can be assumed to be the negative source impedance of a WG divided by the number of WGs. On the other hand, the equivalent impedance of group B can be assumed to be the impedance of an FCL, because it is larger than the impedance of the transmission system and smaller than that of the WGs. Since the equivalent impedance of group B is even smaller than that of group A, the equivalent impedance of the negative-sequence network can be assumed to be the impedance of the FCL.

Consequently, the equivalent impedance of a negative-sequence network can be regard as that of a zero-sequence network, and the following relationship of (18) is valid.

$$\boldsymbol{I}_{Faf}^{-} \times \boldsymbol{K} \approx \boldsymbol{I}_{Faf}^{0} \times \boldsymbol{K}^2 \quad (18)$$

Substituting (18) into (17) gives:

$$\boldsymbol{I}_{Faf}^{+} + 2\boldsymbol{I}_{Faf}^{-} \times \boldsymbol{K} = 0 . \quad (19)$$

In a general case, the coefficient "2" of $|\boldsymbol{I}_{Faf}^{-}|$ can be replaced by scalar coefficient g, i.e.:

$$\boldsymbol{I}_{Faf}^{+} + g\boldsymbol{I}_{Faf}^{-} \times \boldsymbol{K} = 0 , \quad (20)$$

where g is approximately 2, depending on the topologies of the negative- and zero-sequence network.

Consequently, for a DLG fault, the relationship between the fault components at the relaying point can be obtained by:

$$\boldsymbol{I}_{Raf}^{+} + g\boldsymbol{I}_{Raf}^{-} \times \boldsymbol{K} = 0 . \quad (21)$$

Thus,

$$\left|\boldsymbol{I}_{Raf}^{+}\right| = g\left|\boldsymbol{I}_{Raf}^{-}\right|\left|\boldsymbol{K}\right| = g\left|\boldsymbol{I}_{Raf}^{-}\right| > \left|\boldsymbol{I}_{Raf}^{-}\right| . \quad (22)$$

In conclusion, when a DLG fault occurs at F2−F6, $|\boldsymbol{I}_{Raf}^{+}|$ is larger than $|\boldsymbol{I}_{Raf}^{-}|$.

3.2.4 For a 3P fault

When a 3P fault occurs, there are no negative- and zero-sequence components flowing through the fault point. Consequently, there is also no negative-sequence fault component flowing through the relaying point.

Table 2 summarizes the relationships of the symmetrical currents at the fault point and the relaying point for four types of faults. Since the type of fault is evaluated, the faults at F2-F4 can be distinguished from F5/F6 based on the magnitude of the positive-sequence fault component.

Table 2. Relationships of the symmetrical currents at the fault point and the relaying point for four types of faults

Fault type	Currents (Fault point)	Currents (Relaying point)
SLG	$\boldsymbol{I}_{Faf}^{+} = \boldsymbol{KI}_{Faf}^{-} = \boldsymbol{K}^2\boldsymbol{I}_{Faf}^{0}$	$\boldsymbol{I}_{Raf}^{+} = \boldsymbol{KI}_{Raf}^{-}$
LL	$\boldsymbol{I}_{Faf}^{+} + \boldsymbol{KI}_{Faf}^{-} = 0$	$\boldsymbol{I}_{Raf}^{+} + \boldsymbol{KI}_{Raf}^{-} = 0$
DLG	$\boldsymbol{I}_{Faf}^{+} + \boldsymbol{KI}_{Faf}^{-} + \boldsymbol{K}^2\boldsymbol{I}_{Faf}^{0} = 0$	$\boldsymbol{I}_{Raf}^{+} + g\boldsymbol{KI}_{Raf}^{-} = 0$
3P	$\boldsymbol{I}_{Faf}^{-} = \boldsymbol{I}_{Faf}^{0} = 0$	$\boldsymbol{I}_{Raf}^{-} = 0$

Consequently, the WG relay can decide on delayed operation or instantaneous operation.

4. Case Studies

To verify the performance of the proposed algorithm, a WPP is modeled using the EMTP-RV simulator, as shown in Fig. 1. The configuration of the WPP was mentioned in Section 2, and the system frequency is 60 Hz. The sampling rate is 32 samples/cycle, and the voltage and current are passed through the first-order low-pass RC filter with a cutoff frequency of 960 Hz (half the sampling frequency).

The performance of the algorithm is verified under various fault conditions involving changes in the fault positions, the types of faults, and the faulted phases. Results for four of these cases are shown in this paper: an SLG fault at F3, an SLG fault at F1, an SLG fault at F5, and a DLG fault at F5.

4.1 Case 1: A-phase SLG fault at F3 (F3_AG)

Fig. 3 shows the results for this case, where an A-phase SLG fault occurs at Feeder I at 33.33 ms. Fig. 3a indicates the currents, i_{a_WG11} (solid), i_{b_WG11} (dashed), and i_{c_WG11} (dotted), measured at the terminal of WG_{11}. Fig. 3b shows i_{a_WG21}, i_{b_WG21}, and i_{c_WG21}. In Fig. 3c, the solid and dashed

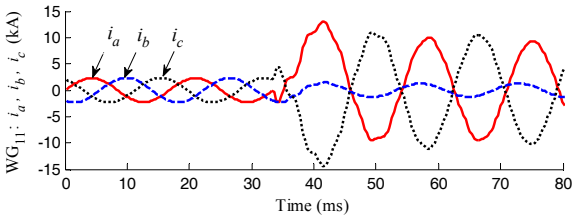

(a) i_{a_WG11} (solid), i_{b_WG11} (dashed) and i_{c_WG11} (dotted)

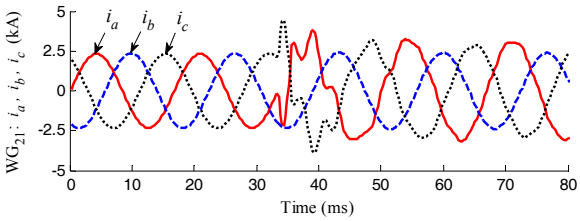

(b) i_{a_WG21} (solid), i_{b_WG21} (dashed) and i_{c_WG21} (dotted)

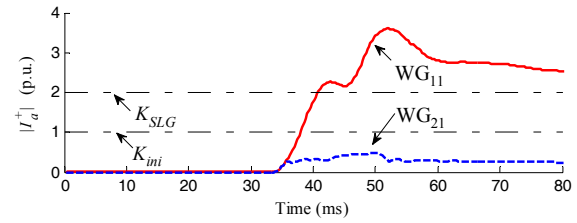

(c) $|\mathbf{I}_{a\_WG11}^{+}|$ (solid) and $|\mathbf{I}_{a\_WG21}^{+}|$ (dashed)

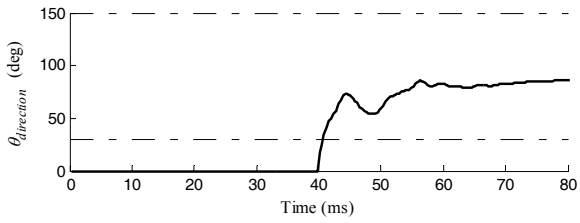

(d) $\theta_{direction}$

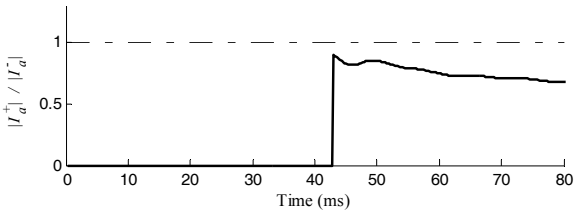

(e) $|\mathbf{I}_{a\_WG11}^{+}|/|\mathbf{I}_{a\_WG11}^{-}|$

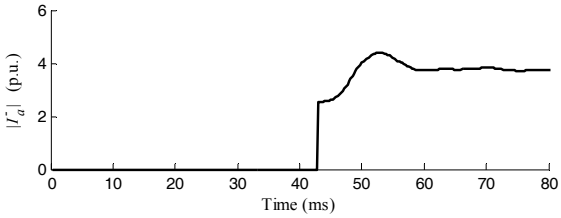

(f) $|\mathbf{I}_{a\_WG11}^{-}|$

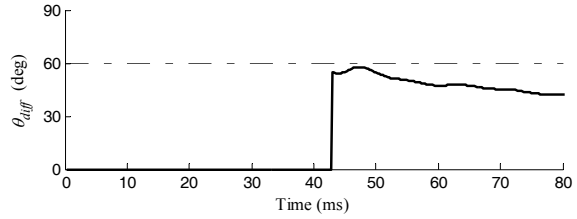

(g) θ_{diff}

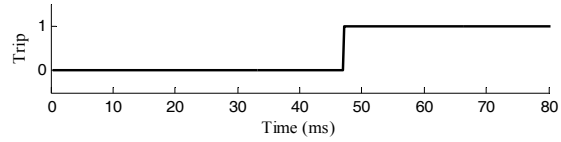

(h) Trip

Fig. 3. Results for F3_AG

lines show $|I_{a\_WG11}^{+}|$ and $|I_{a\_WG21}^{+}|$, respectively, which are shown in per unit quantities.

At stage 1, faults at a parallel WG connected to the same feeder or an adjacent feeder are distinguished from the other faults at a connected feeder, an inter-tie, or a grid. For reliable operation, stage 2 starts if $|I_{a\_WG11}^{+}|$ is larger than K_{ini} for four consecutive samples (2.08 ms). K_{ini}, which is determined via the fault analysis, is set to be 1 in this paper. In this case, $|I_{a\_WG11}^{+}|$ exceeds K_{ini} at 4.69 ms after a fault inception while $|I_{a\_WG21}^{+}|$ does not. This is because $|I_{a\_WG21}^{+}|$ is limited by the large impedance of an FCL and a step-up transformer because a fault occurs at Feeder I. Therefore, WG_{11} relay enters stage 2 at 6.77 ms after a fault inception while the WG_{21} relay remains stable. This means that the proposed protection algorithm does not operate for an adjacent feeder fault.

At stage 2, the fault direction is determined first. In this paper, to avoid maloperation during the transient state, the fault is judged to be a backward fault if $\theta_{direction}$ remains in the region of [30°, 150º] for four consecutive samples. As shown in Fig. 3d, $\theta_{direction}$ enters the operation region at 7.56 ms after a fault inception. Thus, the fault direction is decided as backward at 9.64 ms after a fault inception. In this paper, to determine the fault direction, $\theta_{direction}$ is used only after $|I_{a\_WG11}^{+}|$ exceeds K_{ini}. Thus, $\theta_{direction}$ at stage 2 is shown.

After fault direction determination, to identify the fault type, we check which condition is satisfied among the four conditions in Table 2 for four consecutive samples. For an SLG and an LL fault, $|I_{a\_WG11}^{+}|/|I_{a\_WG11}^{-}|$ is one; for a 3P fault, it is infinite, and for a DLG fault, it is larger than one. In addition, for an SLG fault, θ_{diff} is either 60°, −60°, or 180°, while for an LL fault, θ_{diff} is either 0°, −120°, or 120°.

As mentioned above, for an SLG fault, $|I_{a\_WG11}^{+}|/|I_{a\_WG11}^{-}|$ should be one. However, as shown in Figs. 3c and 3f, $|I_{a\_WG11}^{-}|$ is slightly larger than $|I_{a\_WG11}^{+}|$ after a fault. That is because after the fault inception, $|I_{a\_WG11}^{+}|$ is decreased after reaching its peak value due to the decay of rotor flux whilst $|I_{a\_WG11}^{-}|$ remains stable [17]. Thus, after a fault, $|I_{a\_WG11}^{+}|/|I_{a\_WG11}^{-}|$ is less than one (see Fig. 3e). Hence, it can be judged to be either an SLG or an LL fault. In addition, as shown in Fig. 3g, θ_{diff} slightly decreases as time goes on. However, it is near 60°, so the fault type can be identified as an A-phase SLG fault. This is because the fault type is classified if the condition is satisfied for only four consecutive samples. $|I_{a\_WG11}^{+}|/|I_{a\_WG11}^{-}|$ and θ_{diff} after fault direction determination are shown in Figs. 3e and 3g; note that fault type identification only starts after fault direction determination.

In this paper, the different thresholds corresponding to the four fault types are used to decide on either an instantaneous or delayed trip signal. The threshold values are obtained via the fault analysis. The threshold for an SLG fault, K_{SLG}, is set to be 2. The instantaneous trip signal is activated if $|I_{a\_WG11}^{+}|$ exceeds the threshold for four consecutive samples. $|I_{a\_WG11}^{+}|$ exceeds K_{SLG}, and consequently the instantaneous trip signal is activated at 13.81 ms after a fault inception (see Fig. 3h).

The results indicate that the proposed WG protection relay can operate instantaneously for a connected feeder fault and remain stable for an adjacent feeder fault.

4.2 Case 2: A-Phase SLG fault at F1 (F1_AG)

Fig. 4 shows the results for Case 2, where an A-phase SLG fault occurs at WG_{11} at 33.33ms. In this case, $|I_{a\_WG11}^{+}|$ exceeds K_{ini} at 2.35 ms after a fault inception while $|I_{a\_WG21}^{+}|$ does not, as seen in Fig. 4c. This is because $|I_{a\_WG21}^{+}|$ is significantly limited by the large impedance of

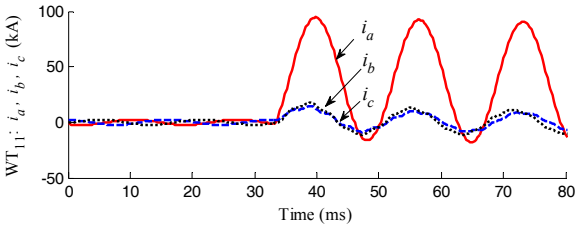

(a) i_{a_WG11} (solid), i_{b_WG11} (dashed) and i_{c_WG11} (dotted)

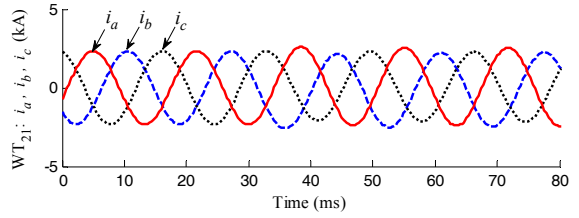

(b) i_{a_WG21} (solid), i_{b_WG21} (dashed) and i_{c_WG21} (dotted)

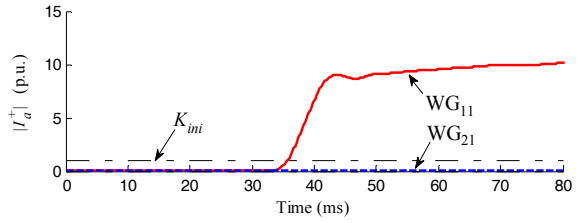

(c) $|I_{a\_WG11}^{+}|$ (solid) and $|I_{a\_WG21}^{+}|$ (dashed)

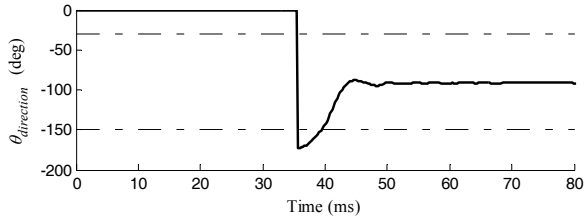

(d) $\theta_{direction}$

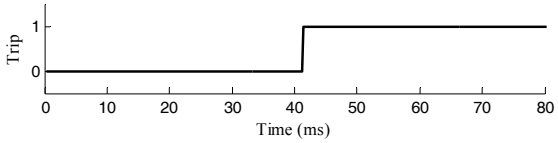

(e) Trip

Fig. 4. Results for F1_AG.

an FCL and step-up transformers because a fault occurs at F1. Therefore, WG_{11} relay enters stage 2 while the WG_{21} relay remains stable.

At stage 2, the fault direction is determined. As shown in Fig. 4d, $\theta_{direction}$ enters the operation region at 6.25 ms after a fault inception. Thus, the fault direction is decided as forward at 8.33 ms after a fault inception. Then, the fault is decided as an internal fault, and the instantaneous operation signal is activated, as shown in Fig. 4e.

The results indicate that for an internal fault of a WG, an instantaneous operation signal is activated successfully.

4.3 Case 3: A-Phase SLG fault at F5 (F5_AG)

Fig. 5 shows the results for Case 2, where an A-phase SLG fault occurs at the inter-tie at 33.33 ms. In this case, the WG_{11} protection relay should operate with a delay. At stage 1, $|\boldsymbol{I}_{a\_WG11}{}^{+}|$ exceeds K_{ini} at 8.08 ms after a fault inception. At stage 2, the proposed protection algorithm identifies the fault as an SLG fault using the same procedure as in Case 1. However, $|\boldsymbol{I}_{a\_WG11}{}^{+}|$ does not exceed K_{SLG} due to the impedance of the main transformer in the substation. Thus, the trip signal is activated at 316.17 ms after a fault inception (Fig. 5f). In this paper, the coordination time is set to be 300 ms, which is commonly used in Korean power system protection.

The results indicate that for an inter-tie fault, a delayed operation signal rather than an instantaneous operation signal is activated successfully.

4.4 Case 4: DLG fault at F5 (F5_BCG)

Fig. 6 shows the results for Case 3; this is identical to Case 2 except for the fault type. At stage 1, $|\boldsymbol{I}_{a\_WG11}{}^{+}|$ exceeds K_{ini} at 5.21 ms after a fault inception, and thus the WG_{11} protection relay enters stage 2.

At stage 2, for a DLG fault, $|\boldsymbol{I}_{a\_WG11}{}^{+}|/|\boldsymbol{I}_{a\_WG11}{}^{-}|$ should be larger than one. As shown in Fig. 6c, a peak exceeding two is seen at 10.42 ms after a fault inception. This is because $|\boldsymbol{I}_{a\_WG11}{}^{-}|$ temporarily reduces to its minimum value, while $|\boldsymbol{I}_{a\_WG11}{}^{+}|$ keeps increasing. $|\boldsymbol{I}_{a\_WG11}{}^{+}|/|\boldsymbol{I}_{a\_WG11}{}^{-}|$ decreases after the peak due to the decrease of $|\boldsymbol{I}_{a\_WG11}{}^{+}|$ but is still larger than one. Thus, the fault type is identified as a DLG fault.

Next, $|\boldsymbol{I}_{a\_WG11}{}^{+}|$ is compared with K_{DLG} instead of K_{SLG}, which is set to be 3.5 in this paper. As seen in Fig. 6b, $|\boldsymbol{I}_{a\_WG11}{}^{+}|$ does not exceed K_{DLG}. Consequently, the trip signal is activated at 312.27 ms after a fault inception, considering the 300 ms coordination time (Fig. 6e).

The results indicate that the proposed WG protection relay can successfully distinguish between an instantaneous and delayed operation, irrespective of the type of fault.

5. Hardware Implementation

This Section shows the results obtained when the proposed WG protection algorithm was implemented on a hardware platform based on a TMS320C6701 DSP (Fig. 7).

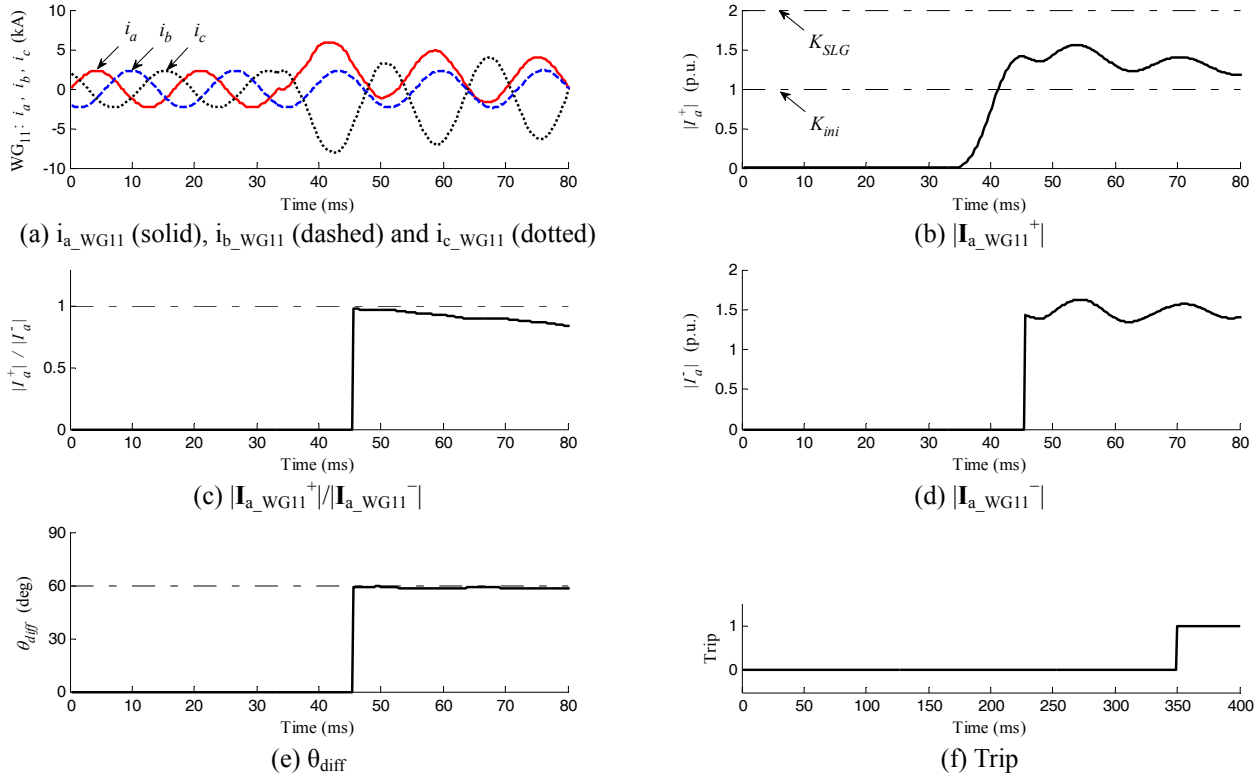

(a) i_{a_WG11} (solid), i_{b_WG11} (dashed) and i_{c_WG11} (dotted)

(b) $|\mathbf{I}_{a\_WG11}{}^{+}|$

(c) $|\mathbf{I}_{a\_WG11}{}^{+}|/|\mathbf{I}_{a\_WG11}{}^{-}|$

(d) $|\mathbf{I}_{a\_WG11}{}^{-}|$

(e) θ_{diff}

(f) Trip

Fig. 5. Results for F5_AG

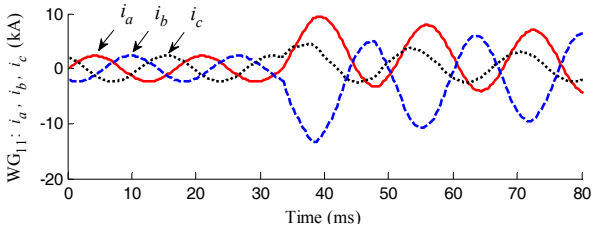

(a) i_{a_WG11} (solid), i_{b_WG11} (dashed) and i_{c_WG11} (dotted)

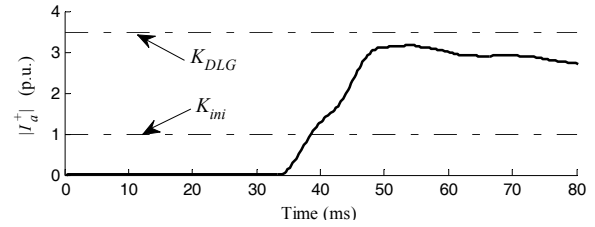

(b) $|\boldsymbol{I}_{a\_WG11}{}^{+}|$

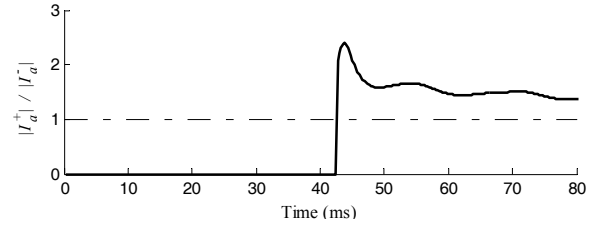

(c) $|\boldsymbol{I}_{a\_WG11}{}^{+}|/|\boldsymbol{I}_{a\_WG11}{}^{-}|$

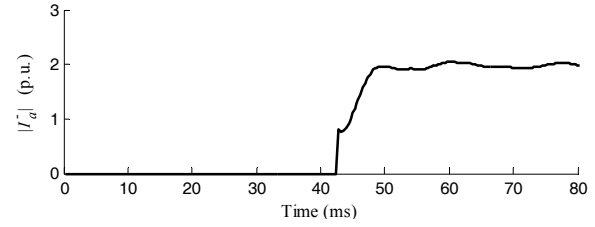

(d) $|\boldsymbol{I}_{a\_WG11}{}^{-}|$

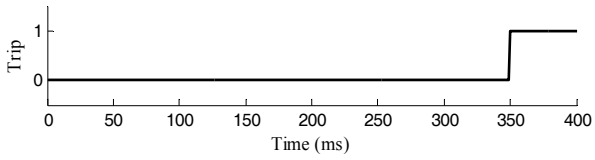

(e) Trip

Fig. 6. Results for F5_BCG

The three voltages and three currents generated by EMTP-RV are converted into analog signals using a PCI 1724 U D/A board. The signals are then passed through first-order RC filter (f_c = 960 Hz) to the 16-bit A/D converters operating at a sampling rate of 32 s/c.

Fig. 8 shows the results obtained when the hardware implementation was evaluated using the voltage and current signals described in Case 1. The results are very similar to those shown in Fig. 3 and as expected the proposed relay operates instantaneously and the trip signal is activated.

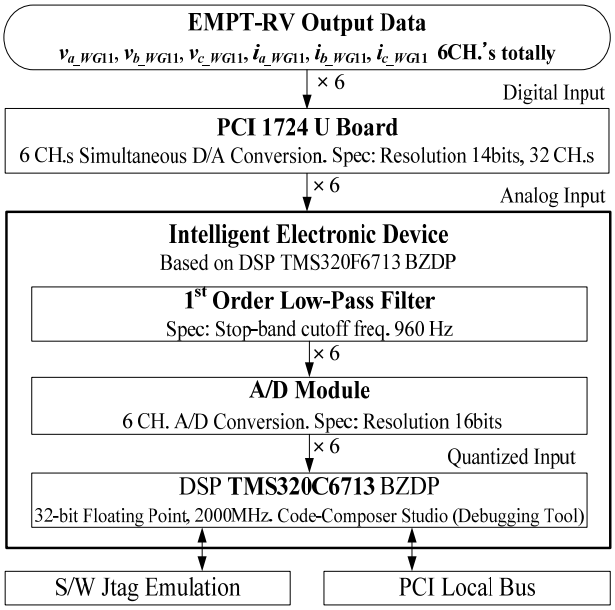

Fig. 7. Configuration of hardware implementation

6. Conclusions

A WG protection relay based on the positive- and negative-sequence fault components is proposed in this paper. At stage 1, faults requiring an instantaneous or delayed operation are discriminated from those requiring non-operation based on the magnitude of the positive-sequence fault component. At stage 2, after fault direction determination, either instantaneous or delayed operation is decided based on fault type classification using the relationships between the positive- and negative-sequence fault components.

The performance of the proposed WG protection relay was verified using EMTP-RV generated data. The results indicate that the proposed protection relay can successfully distinguish among instantaneous, delayed, or non-operation for fault positions, irrespective of the type of fault and the faulted phases. To investigate the feasibility of building a commercial relay, a prototype relay was constructed using a DSP based hardware platform and tested using a relay test set. Results described in the paper, show that a prototype relay, based on the described protection algorithm, successfully operate instantaneously for a connected feeder fault.

This paper shows only the results for a WPP consisting of induction generators. However, for a WPP consisting of other types of generators, a WG protection relay should be developed considering the characteristics of the WGs during the transient state. The proposed relay can minimize the outage zone and thus undesirable disconnection of WPPs or healthy WGs can be avoided.

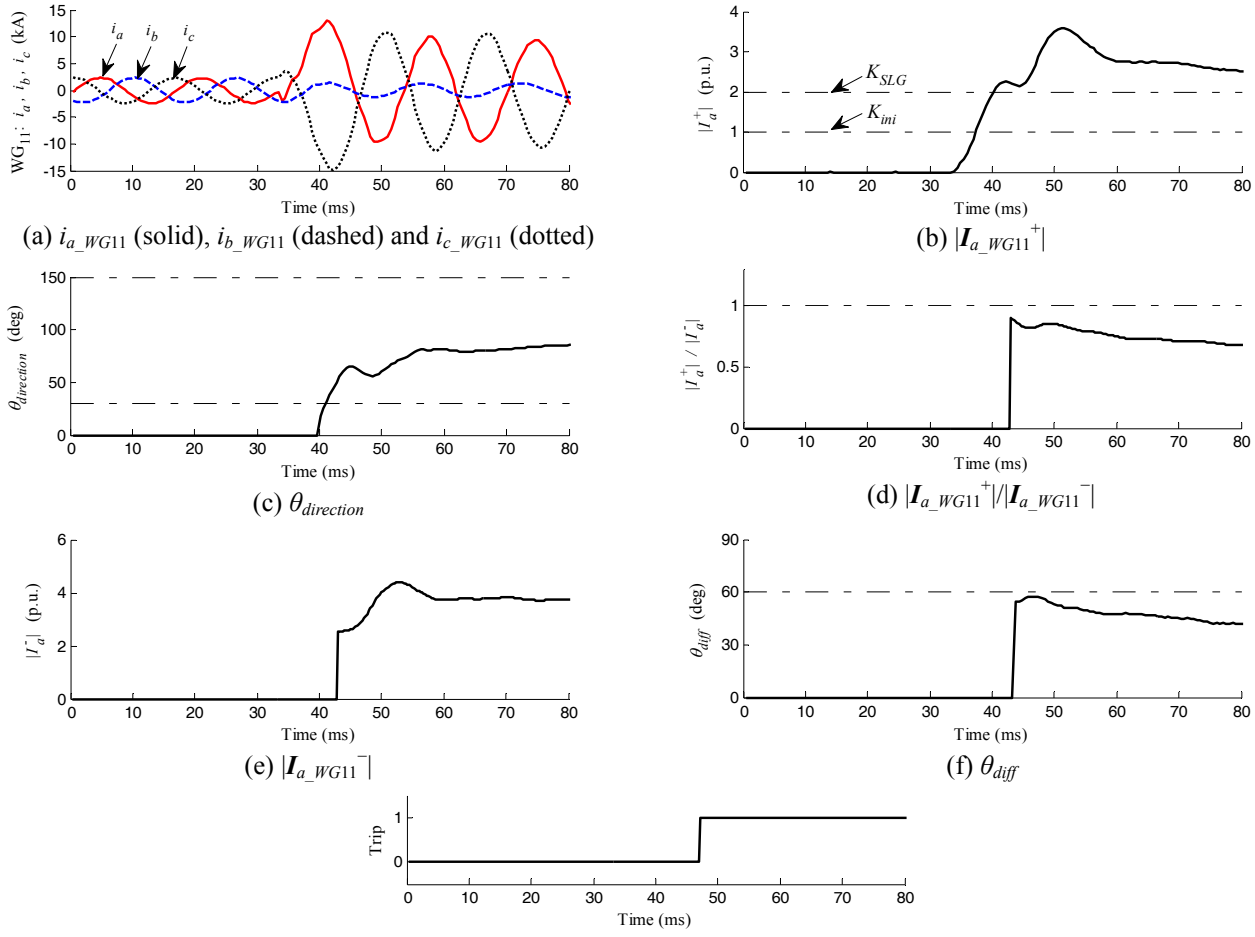

Fig. 8. Results for F3_AG

Acknowledgements

This work was supported by the National Research Foundation of Korea (NRF) grant funded by the Korea government (MSIP) (2012-0009146).

References

[1] Cable News Network (CNN). Clinton hails global warming pact. [Online]. Available: http://www.cnn.com/ALLPOLITICS/1997/12/11/kyoto/

[2] The energy report: 100% renewable energy by 2050. World wildlife fund, Washington, DC, USA. [Online]. Available: http://www.worldwildlife.org

[3] World wind energy report 2010. World wind energy association, Bonn, Germany. [Online]. Available: http://www.wwindea.org

[4] Steven J Haslam, Peter A Crossley and Nicholas Jenkins, "Design and field testing of a source based protection relay for wind farms," *IEEE Trans. on Power Deliv.*, vol. 14, no. 3, pp. 818-823, Jul. 1999.

[5] Steven J Haslam, Peter A Crossley and Nicholas Jenkins, "Design and evaluation of a wind farm protection relay," *IEE Proc. -Gener. Transm. Distrib.*, vol. 146, no. 1, pp. 37-44, Jan. 1999.

[6] Shenghu Li, Shasha Sun and Shaofei Li, "Operation characteristics of zone 3 impedance relays in wind power systems with fixed-speed induction generators," in *2011 Asia-Pacific Power and Energy Engineering Conference*, Wuhan, China, Mar. 2011.

[7] GE Consumer & Industrial Multilin, W650-Wind generator protection system instruction manuals, 2006 GE Multilin. [online]. Available: http://www.gedigitalenergy.com/app/ViewFiles.aspx?prod=w650&type=3

[8] Schweitzer Engineering Laboratories, SEL-700GW wind generator relay. [online]. Available: http://www.selinc.com/sel-700gw/

[9] Taiying Zheng, Yeon-Hee Kim and Yong Cheol Kang, "Protection for a wind turbine generator in a large wind farm," *Journal of Electrical Engineering & Technology*, vol. 6, no. 4, pp. 466-473, Jul. 2011.

[10] Taiying Zheng, Seung-Tae Cha, Byung-Eun Lee, Peter A Crossley, Minho Song and Yong Cheol Kang, "Design and evaluation of a protection algorithm for a wind turbine generator based on the fault generated

symmetrical components," *IEEE PES Innovative Smart Grid Technologies Europe 2011*, Manchester, UK, Dec. 2011.
[11] Lin Ye and Liang Zhen Lin, "Study of superconducting fault current limiters for system integration of wind farms," *IEEE Trans. on Applied Superconductivity*, vol. 20, no. 3, pp. 1233-1237, Jun. 2010.
[12] Eduard Muljadi, Vahan Gevorgian and Francisco Delarosa, "wind power plant enhancement with a fault current limiter," in *Proc. 2011 IEEE Power and Energy Society General Meeting*, Detroit, MI, USA, Jul. 2011.
[13] Michael Reichard, Dale Finney and John Garrity, "Wind farm system protection using peer-to-peer communications," in *Proc. IEEE 6th Annu. Conf. Protective Relay Eng.*, TX, USA, Mar. 2007.
[14] Wind Plant Collector Design WG, "Wind power plant grounding, overvoltage protection, and insulation coordination," in *Proc. 2009 IEEE Power and Energy Society General Meeting*, Calgary, Canada, Jul. 2009.
[15] Houlei Gao and Peter A Crossley, "Design and evaluation of a directional algorithm for transmission-line protection based on positive-sequence fault components," *IEE Proc. -Gener. Transm. Distrib.*, vol. 153, no. 6, pp. 711-718, Nov. 2006.
[16] J. Lewis Blackburn and Thomas J. Domin, *Protective relaying principles and applications*: 3rd ed., CRC Press, Taylor & Francis Group, LLC, 2007.
[17] V. Gevorgian, M. Singh, and E. Muljadi, "Symmetrical and unsymmetrical fault currents of a wind power plant," in *2012 IEEE Power and Energy Society General Meeting*, San Diego, California USA, Jul. 22-26, 2012.

Taiying Zheng He received his B.S., M.S., and Ph.D. degrees from Zhejiang University, China, in 2004, and Chonbuk National University, Korea, in 2006 and 2011, respectively. From 2011 to 2012 He was a research professor in the Wind Energy Grid-Adaptive Technology Center, Korea. Now he is a research associate in the University of Manchester, UK. His research interests are the development of protection systems for power systems and new protection/control systems for wind farms.

Seung-Tae, Cha He received his B.S degree in Electrical Engineering from Illinois Institute of Technology, Chicago, U.S. in 1992, and M.S degree in Electrical Engineering from Yonsei University, Korea in 1997. He is a Ph. D candidate at Technical University of Denmark & Korea University. His research interest includes real-time simulation of power systems, integration of renewable energy, model development, studies involving load flow, system planning & operation.

Yeon-Hee Kim He received his B.S. and M.S. degrees from Chonbuk National University, Korea, in 2006 and 2008, respectively. He is currently pursuing a Ph.D. degree from Chonbuk National University, Korea. He is also an assistant researcher at the WeGAT Research Center. His research interest is the development of new control/protection systems for wind power plants and power systems using digital signal processing techniques.

Peter A. Crossley He was born in the U.K. in 1956. He received the B.Sc. degree from the University of Manchester (formerly UMIST), Manchester, U.K., in 1977 and the Ph.D. degree from the University of Cambridge, Cambridge, U.K., in 1983. He is a Professor of Electrical Engineering at the University of Manchester. He is an active member of various CIGRE, IEEE, and IET committees on protection and control.

Sang Ho Lee He received his B.S., M.S., and Ph.D. degrees from Seoul National University, Korea, in 1995, 1997, and 2003, respectively. He has been with Korea Electrotechnology Research Institute (KERI), Korea, since 2003. He is currently a senior researcher at KERI, Korea. His research interests are the development of an energy management system for power system and wind farms, and optimal operating schemes for the smart grid.

Yong Cheol Kang He received his B.S., M.S., and Ph.D. degrees from Seoul National University, Korea, in 1991, 1993, and 1997, respectively. He has been with Chonbuk National University, Korea, since 1999. He is currently a professor at Chonbuk National University, Korea, and the director of the WeGAT Research Center. He is also with the Smart Grid Research Center at Chonbuk National University. His research interests are the development of new protection and control systems for wind power plants and the enhancement of wind energy penetration levels by keeping the capacity factor of wind generators high.